Dyes and Pigments 163 (2019) 660–666

Contents lists available at ScienceDirect

Dyes and Pigments

journal homepage: www.elsevier.com/locate/dyepig

# Synthesis of new conjugated small-molecule-dyes based on 2-(2-methyl-4*H*-chromen-4-ylidene)malononitrile as the electron-withdrawing group and their application in photovoltaic devices

Dong Geun Kim[a,1], Ho Cheol Jin[a,1], Ratna Dewi Maduwu[a], Sabrina Aufar Salma[a], Doo Kyung Moon[b], Joo Hyun Kim[a,*]

[a] Department of Polymer Engineering, Pukyong National University, Busan, 48547, South Korea
[b] Department of Materials Chemistry and Engineering, Konkuk University, Seoul, 05029, South Korea

ARTICLE INFO

*Keywords:*
Conjugated molecule
2-(2-methyl-4*H*-chromen-4-ylidene) malononitrile
Organic solar cell

ABSTRACT

A series of new acceptor-donor-acceptor (A-D-A) type conjugated small-molecule-dyes based on indacenodithieno[3,2-*b*]thiophene (**IDTT**) and 2-(2-methyl-4*H*-chromen-4-ylidene)malononitrile (**CMCN**), named **IDTT-CMCN** and **IDTT-HT-CMCN**, have been synthesized for application in organic solar cells. A-D-A type small-molecules with **CMCN** can effectively form a powerful push-pull structure that induces effective intramolecular charge transport (ICT) and enhanced optical absorption. In comparison with **IDTT-CMCN**, **IDTT-HT-CMCN** has 3-hexylthiophene (**HT**) as a π-bridge unit between the **IDTT** and **CMCN** moieties to increase the solubility and extend the π-conjugation length. The resulting dye (**IDTT-HT-CMCN**) with a hexylthiophene ring as a π-bridge showed a smaller band gap and better solubility. Thus, a power conversion efficiency (PCE) as high as 7.60% was achieved with a short circuit current of 12.7 mA/cm$^2$, open circuit voltage of 0.94 V, and fill factor of 63.8%. To the best of our knowledge, small-molecule-based donors with **CMCN** as an electron-withdrawing unit have never been reported before. In addition, the PCE of 7.60% reported in this work is highly efficient among the PCE reported for an organic solar cell using an **IDTT**-based small-molecule-donor material.

## 1. Introduction

Solution-processed organic solar cells (OSCs) based on bulk heterojunction (BHJ) structures [1] composed of blended conjugated electron donors and acceptors have attracted considerable attention as electricity-generating devices due to their unique properties such as their light weight, mechanical flexibility, and low-cost fabrication over large areas [2,3]. Over the last few decades, the development of conjugated polymers and small molecules as p-type organic semiconductors has led to the progressive enhancements of device performances, with power conversion efficiencies (PCEs) now reaching over 10% [4–7]. Compared to polymeric donors, small molecule donors in OSCs possess intrinsic advantages, including monodispersity, a well-defined and versatile structure, and no batch-to-batch variations [8,9]. In recent years, small molecule-based donors having an acceptor-donor-acceptor (A-D-A) architecture with π-bridge units have shown great potential for applications in OSCs. The optical and electrochemical properties of A-D-A small molecule donors can be easily tuned by using different donating and accepting units, which can also enable efficient intramolecular charge transport (ICT) within D-A moieties [10].

Many electron-donating units such as benzodithiophene (BDT) [11–16], dithienosilole(DTS) [17–20], or oligothiophene [21,22] have been investigated for the design of ideal molecular structures with the goal to produce high photovoltaic performance. So far, p-type small molecules based on those electron donating units have shown high PCEs up to 11.3% in single-junction OSCs [23]. Though various electron donating units have been applied to the synthesis of small molecules, indacenodithieno[3,2-*b*]thiophene (**IDTT**) is a promising candidate for the central building block in A-D-A small molecules owing to its coplanar structure and extended backbone, which is beneficial to enhancing π-electron delocalization, light harvesting, and hole mobility [24]. In addition, four bulky side chains on the **IDTT** backbone prevent strong self-aggregation, so that **IDTT**-based molecules have better solubility in common organic solvents and form a favorable morphology [25]. These molecules are listed in Table S1, which provides a summary of small-molecule-based OSCs with reported PCEs over 6%. Using **IDTT**

* Corresponding author.
*E-mail address:* jkim@pknu.ac.kr (J.H. Kim).
[1] D. G. Kim and H. C. Jin equally contributed to this research.

https://doi.org/10.1016/j.dyepig.2018.12.060
Received 7 November 2018; Received in revised form 26 December 2018; Accepted 26 December 2018
Available online 27 December 2018
0143-7208/ 

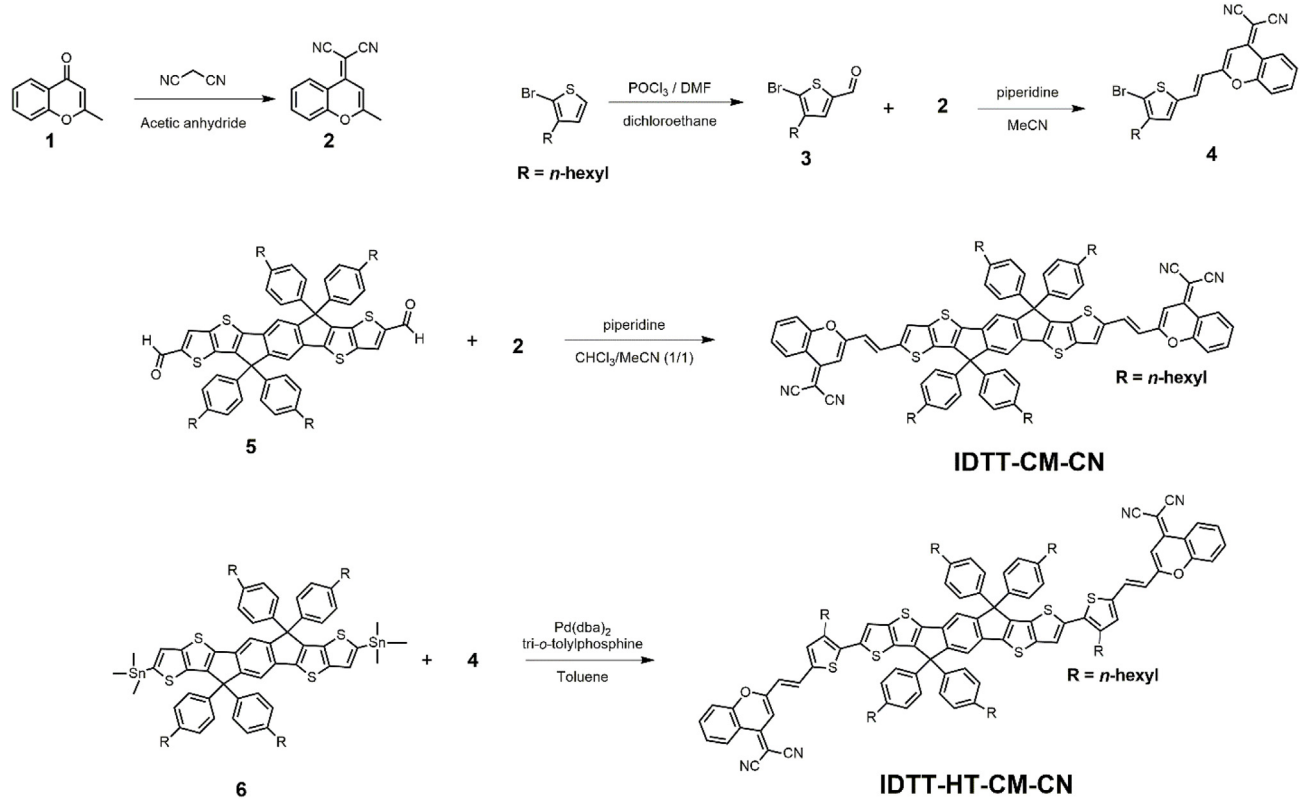


**Scheme 1.** Chemical structures of **IDTT-CMCN** and **IDTT-HT-CMCN**.

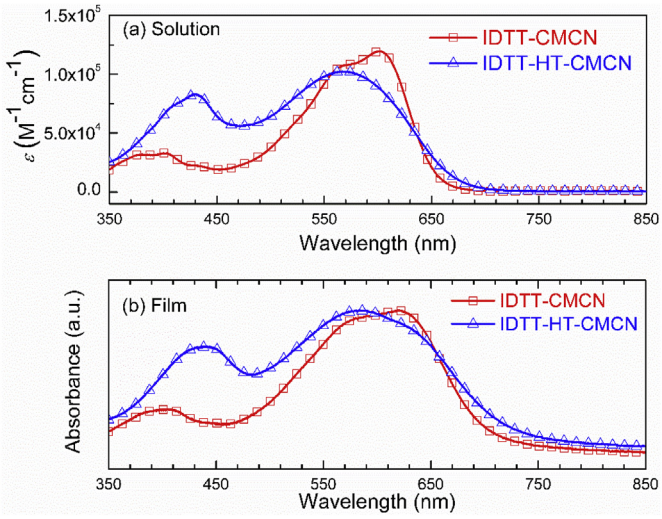


**Fig. 1.** UV–visible spectra of **IDTT-CMCN** and **IDTT-HT-CMCN** (a) solutions in chloroform and (b) films on glass substrates.

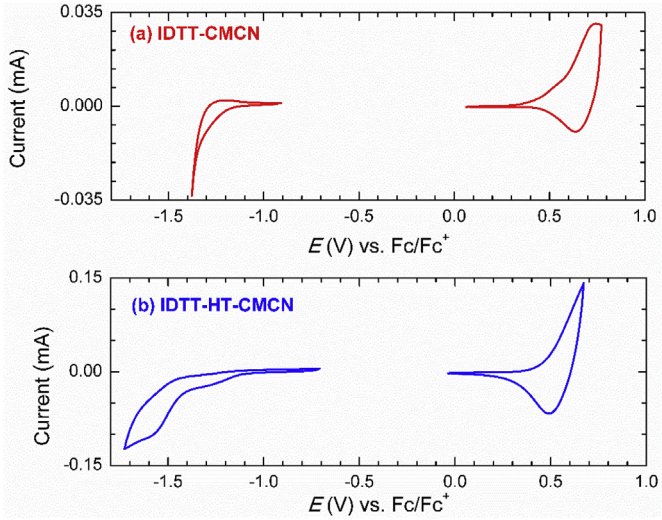


**Fig. 2.** Cyclic voltammograms of (a) **IDTT-CMCN** and (b) **IDTT-HT-CMCN**.

units with various strong electron-withdrawing units for A-D-A small molecule acceptors such as ITIC has been successfully demonstrated in previous reports [26]. The devices based on those acceptors with a polymeric donor showed excellent performance with greater than 11% efficiency [27–35]. Unlike the application of **IDTT** units as acceptors, there have been few reports for the application of small molecule donors in OSCs [36,37], while devices with **IDTT**-based donors and fullerene acceptors have been reported with a PCE of up to 7.05% [38].

For the design of A-D-A small molecule donors containing **IDTT** as the electron donating unit, it is necessary to develop end-capping units with proper energy levels to match the electron acceptors and thus improve photovoltaic performance. From this perspective, the carbonyl

**Table 1**
Summary of optical and electrochemical properties of **IDTT-CMCN** and **IDTT-HT-CMCN**.

| | $\lambda_{edge}$(nm)[a]<br>$E_{gap}^{opt}$(eV)[b] | $\lambda_{max}^{solution}$ (nm)<br>$\lambda_{max}^{film}$ (nm) | HOMO (eV)[c] | LUMO (eV)[d] |
|---|---|---|---|---|
| **IDTT-CMCN** | 700<br>1.77 | 400, 601<br>400, 620 | −5.33 | −3.49 |
| **IDTT-HT-CMCN** | 724<br>1.71 | 430, 569<br>439, 583 | −5.27 | −3.43 |

[a] Absorption edge of the film.
[b] Estimated from the $\lambda_{edge}$.
[c,d] Estimated from the CV.

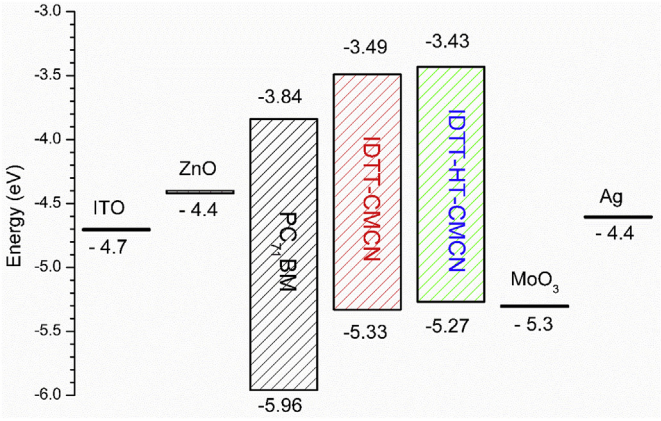


**Fig. 3.** Energy level diagrams of **IDTT-CMCN**, **IDTT-HT-CMCN** and the materials used in this research.

oxygen of chromone (**CM**) derivatives can be replaced with ylidene malononitrile, 2-(2-methyl-4H-chromen-4-ylidene)malononitrile (**CMCN**), to yield ideal end-capping unit because of their strong electron accepting nature and planar structure. **CMCN** derivatives have been used for red-emitting dyes and as dopants in organic light emitting diodes (OLEDs) [39,40]. However, they are rarely applied as photoactive materials in OSCs. When **CMCN** derivatives are introduced to the electron donating units in A-D-A small molecules, they can effectively form a powerful push-pull structure that induces effective ICT and enhanced optical absorption.

Herein, we designed and synthesized two A-D-A small molecule donors, denoted as **IDTT-CMCN** and **IDTT-HT-CMCN**, containing **IDTT** as the electron donating unit and **CMCN** as the electron-withdrawing unit. In comparison with **IDTT-CMCN**, **IDTT-HT-CMCN** has 3-hexylthiophene (**HT**) as a π-bridge unit between the **IDTT** and **CMCN** moieties to increase the solubility and extend the π-conjugation length. OSCs based on both of these donors and [6,6]-phenyl-C71-butyric acid methyl ester ($PC_{71}BM$) as the acceptor were fabricated to investigate the effect of alkylthiophenes on the photovoltaic properties. Consequently, **IDTT-HT-CMCN** exhibits stronger absorption of the short wavelength region than that of **IDTT-CMCN** and favorable film morphology when blended with $PC_{71}BM$. To the best of our knowledge, small-molecule-based donors with **CMCN** as an electron-withdrawing unit have never been reported before. In addition, the PCE of 7.60% achieved in this research is the highest PCE reported for OSCs using the **IDTT**-based small-molecule donors.

## 2. Results and discussion

### 2.1. Synthesis and thermal properties

The detailed synthetic routes of the materials are illustrated in Scheme 1. Compound **4** was synthesized by a condensation reaction between compounds **2** and **3** in the presence of piperidine as a catalyst in acetonitrile (ACN), giving a yield of over 40%. Synthesis of **IDTT-CMCN** was followed by similar procedures for the synthesis of compound **4**. However, a mixed solvent of chloroform (CF) and ACN was used to synthesize **IDTT-CMCN** because of its poor solubility in ACN. **IDTT-CMCN** showed moderated solubility in CF (up to 5 mg/mL) but poor solubility in toluene, chlorobenzene (CB), and *o*-dichlorobenzene (DCB). **IDTT-HT-CMCN** was prepared by the Stille coupling reaction between compounds **4** and **6**. **IDTT-HT-CMCN** showed better solubility in CF (up to 10 mg/mL) due to the hexyl group on the thiophene ring also exhibited poor solubility in toluene, CB, and DCB. Thermogravimetric analysis (TGA) of **IDTT-CMCN** and **IDTT-HT-CMCN** was carried out at a heating rate of 10 °C/min under air atmosphere (See Fig. S1). **IDTT-CMCN** and **IDTT-HT-CMCN** showed good thermal stability with the onset of decomposition temperatures of 407 and 393 °C at 5 wt % loss, respectively. Differential scanning calorimetry (DSC) thermograms of **IDTT-CMCN** and **IDTT-HT-CMCN** are displayed in Fig. S2. No discernible thermal transitions such as melting or glass transition were detected during the heating processes up to 300 °C, due to their amorphous properties.

### 2.2. Optical and electrochemical properties

As shown in Fig. 1 **(a)**, the UV–Vis spectra of both **IDTT-CMCN** and **IDTT-HT-CMCN** solutions exhibit two absorption bands in the shorter (350–470 nm) and longer wavelength regions (470–670 nm), respectively. The former corresponds to the π-π* transition of the conjugated backbone and the latter corresponds to ICT, which is generally observed

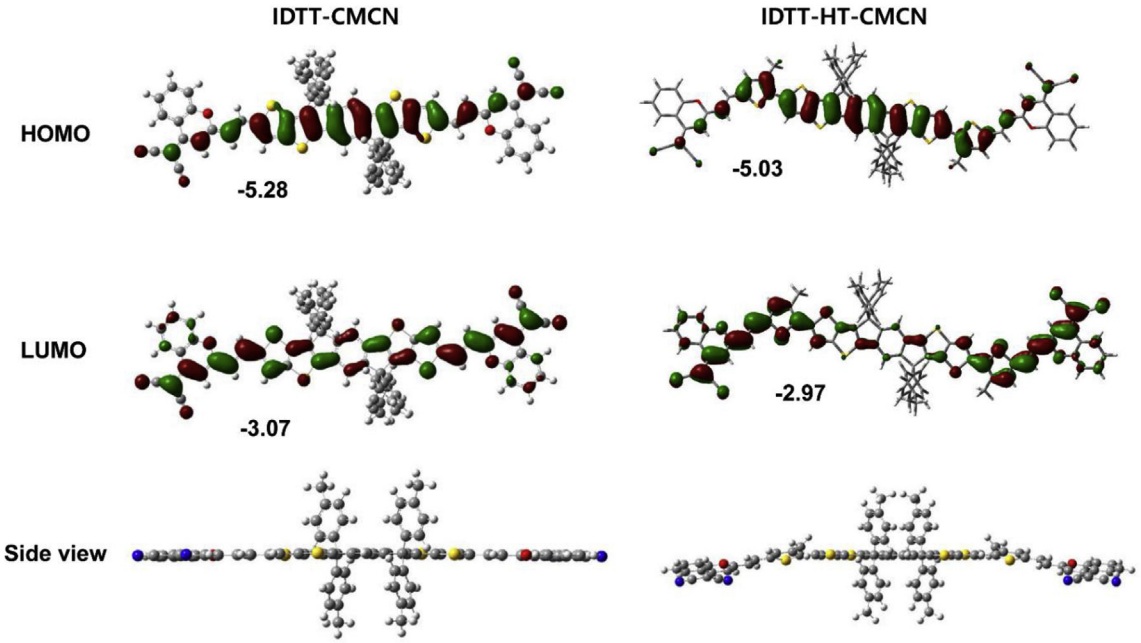


**Fig. 4.** Calculated frontier molecular orbitals of **IDTT-CMCN** and **IDTT-HT-CMCN** with HOMO/LUMO energy levels.

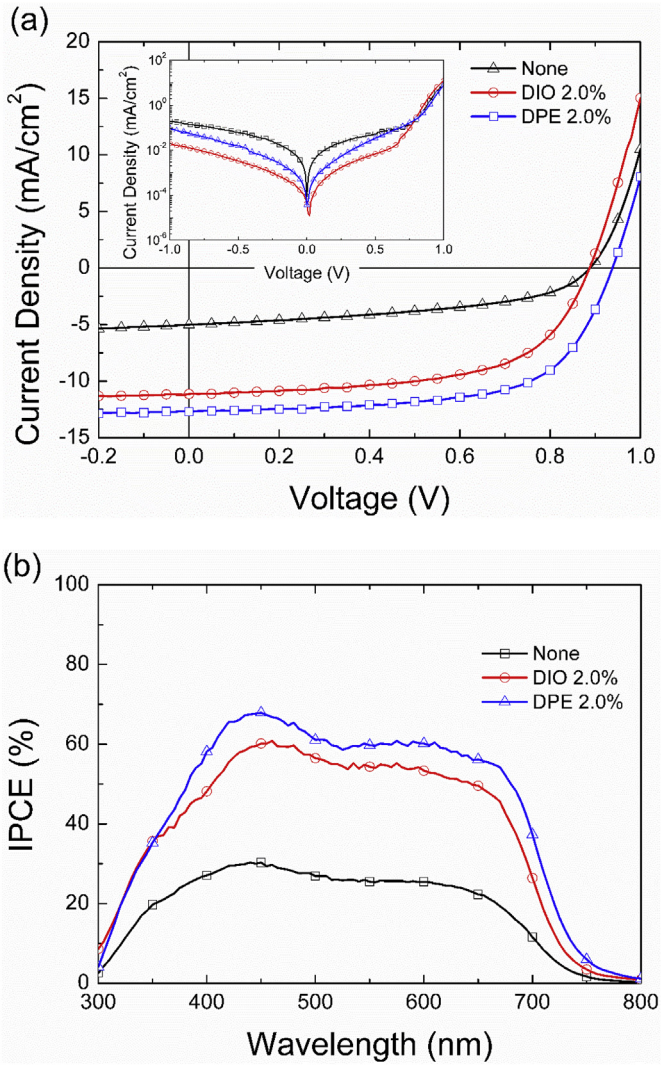


**Fig. 5.** (a) Current density vs. voltage curves of OSCs under 1.0 sun illumination (inset: under dark conditions) and (b) IPCE spectra of OSCs based on **IDTT-HT-CMCN**.

in conjugated materials with a donor and acceptor architecture. The maximum wavelength corresponding to the π-π* transition of **IDTT-HT-CMCN** is 430 nm, which is longer than that of **IDTT-CMCN** (400 nm). This is due to the extended π-conjugation length resulting from the insertion of a thiophene ring between **IDTT** and **CMCN**. On the other hand, the maximum position of the ICT band of **IDTT-HT-CMCN** (569 nm) appeared at a shorter wavelength than that of **IDTT-CMCN** (601 nm). This is possibly due to the fact that the ICT in **IDTT-CMCN** is stronger than that in **IDTT-HT-CMCN** [32]. The molar extinction coefficient ($\varepsilon$) of **IDTT-CMCN** at 601 nm is $1.2 \times 10^5\ M^{-1}\ cm^{-1}$, which is higher than that of **IDTT-HT-CMCN** ($1.0 \times 10^5\ M^{-1}\ cm^{-1}$) at 569 nm. The higher $\varepsilon$ of **IDTT-CMCN** supports the observation that ICT is stronger in **IDTT-CMCN**. The UV–Vis spectra of **IDTT-CMCN** and **IDTT-HT-CMCN** films (Fig. 1 **(b)**) showed similar features to those of the solution phase spectra. The values of the maximum wavelength of the π-π* transition, $\lambda_{edge}$, and $E_{gap}^{opt}$ of **IDTT-HT-CMCN** are 439 nm, 724 nm, and 1.71 eV, respectively, which are red-shifted compared with those of **IDTT-CMCN** (400 nm, 700 nm, 1.77 eV). This is due to an increase in the number of thiophene rings in **IDTT-HT-CMCN**. The positions of the ICT bands of **IDTT-CMCN** and **IDTT-HT-CMCN** exhibited similar trends in their solution spectra. The position of the absorption peaks of the films are red-shifted compared with those of the solutions owing to the intermolecular π-π stacking.

The HOMO energy level of **IDTT-HT-CMCN,** as determined from the oxidation onset potential of the corresponding cyclic voltammogram (CV) (Fig. 2), was −5.27 eV, which is higher than that of **IDTT-CMCN** (−5.33 eV) owing to the incorporation of a thiophene ring into **IDTT-HT-CMCN**. The LUMO energy levels of **IDTT-CMCN** and **IDTT-HT-CMCN** calculated from the reduction onset potential of the corresponding CVs were −3.49 and −3.43 eV, respectively. The optical and electrochemical properties of **IDTT-CMCN** and **IDTT-HT-CMCN** are summarized in Table 1.

Energy level diagrams of **IDTT-CMCN**, **IDTT-HT-CMCN**, and other materials in the OSC are illustrated in Fig. 3. From the energy levels, facile exciton dissociation from the donor to $PC_{71}BM$ as well as an energetically favored charge transfer process can be expected.

### 2.3. Theoretical calculations

Computational calculations based on density functional theory (DFT) were employed to determine the optical and electrochemical properties. The DFT calculations were performed using Gaussian 09 software with the hybrid B3LYP correlation functional and split valence 6-31G(d) basis set. Due to the limits of calculation, the hexyl side chains on **IDTT** and thiophene were replaced with methyl groups. The optimized geometries of **IDTT-CMCN** and **IDTT-HT-CMCN** are displayed in Fig. 4. The HOMO orbitals are delocalized in the conjugated backbone. On the other hand, the LUMO orbitals are localized in the CMCN unit. The calculated HOMO/LUMO levels of **IDTT-CMCN** and **IDTT-HT-CMCN** are −5.28/-3.07 and −5.03/-2.97, respectively. Even though these values do not exactly match those observed in the UV–Vis spectra and CVs, they are well correlated with the experimental results. It can be shown that the shoulder observed in the absorption peak around 620 nm in the UV–Vis spectra of **IDTT-CMCN** and **IDTT-HT-CMCN** is due to the formation of intermolecular aggregates. It is very interesting that this shoulder peak in the spectrum of **IDTT-CMCN** is stronger than that of **IDTT-HT-CMCN**. Based on the side view of **IDTT-CMCN** and **IDTT-HT-CMCN** in Fig. 4, **IDTT-CMCN** shows a more planar structure than **IDTT-HT-CMCN**. The theoretical calculations also provide a good interpretation for the aggregation observed in the film state. This supports the observation that the solubility of **IDTT-CMCN** is poor

**Table 2**
The best photovoltaic parameters of the OSCs based on **IDTT-HT-CMCN** at the blend ratio of 3:8 (w/w) between **IDTT-HT-CMCN** and $PC_{71}BM$. The averages and error range for the photovoltaic parameters of each device are given in parentheses.

| Additive[a] | $J_{sc}$ (mA/cm$^2$) | Calculated $J_{sc}$[b] (mA/cm$^2$) | $V_{oc}$ (V) | FF (%) | PCE (%) | $R_s$[c] (Ω cm$^2$) |
|---|---|---|---|---|---|---|
| none | 5.01 (4.91 ± 0.08) | 5.24 | 0.89 (0.88 ± 0.01) | 47.3 (46.5 ± 0.70) | 2.11 (2.02 ± 0.06) | 4.52 |
| DIO 2.0% | 11.1 (11.0 ± 0.03) | 10.9 | 0.89 (0.89 ± 0.01) | 59.9 (59.8 ± 0.31) | 5.93 (5.91 ± 0.02) | 3.97 |
| DPE 2.0% | 12.7 (12.2 ± 0.33) | 12.6 | 0.94 (0.94 ± 0.01) | 63.8 (63.6 ± 0.8) | 7.60 (7.27 ± 0.21) | 3.75 |

[a] Thickness of the active layer was 50 nm.
[b] Calculated from the IPCE curves.
[c] Series resistance estimated from the device showing the best PCE.

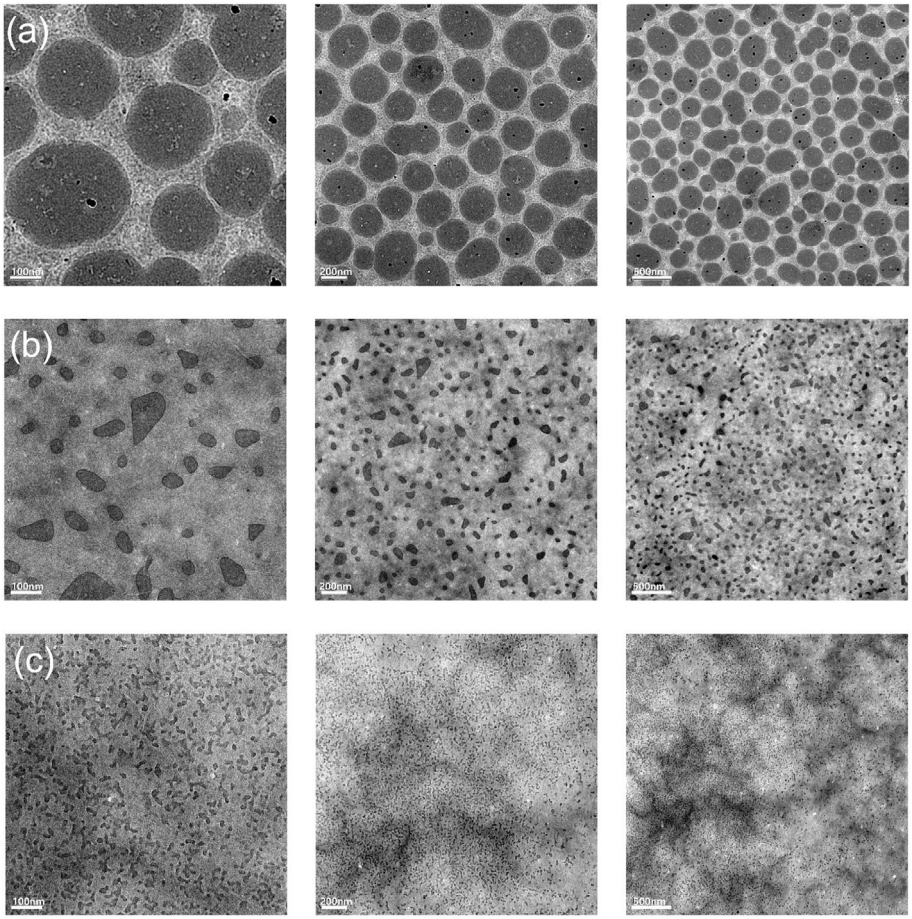


**Fig. 6.** TEM images of the active layers based on **IDTT-HT-CMCN** at various magnification (a) without additive, (b) with 2.0% DIO, and (c) 2.0% DPE.

compared to that of **IDTT-HT-CMCN**.

### 2.4. Photovoltaic properties

To evaluate the performance of **IDTT-CMCN** and **IDTT-HT-CMCN** as the donor in OSCs, we fabricated and tested inverted type polymer solar cells (PSCs) with a structure of ITO/ZnO (15 nm)/donor:$PC_{71}BM$/$MoO_3$ (10 nm)/Ag (100 nm). Devices based on **IDTT-CMCN** with different blend ratios of donor and $PC_{71}BM$ from 3:7 to 3:9 (w/w) were fabricated and tested to optimize the device fabrication conditions; we fabricated OSCs with diphenyl ether (DPE) as a processing additive as well. The current density-voltage (*J-V*) curves of the OSCs under AM 1.5G simulated illumination and the photovoltaic parameters are shown in Fig. S3 and Table S2. The PCEs were around 0.25–0.45%. Regardless of the blend ratio of the active layer, the devices containing DPE as a processing additive exhibited decreased PCEs. This is due to the morphology of the active layer. As shown in TEM images (Fig. S4), no discernible morphological changes were observed in the active layer with processing additive. One reason for this is the poor solubility of **IDTT-CMCN** in CF (up to 5 mg/mL in CF). It should be noted that the photovoltaic results achieved for devices based on **IDTT-CMCN** do not provide us with important information. OSCs based on **IDTT-HT-CMCN** as the donor with different blend ratios of donor and $PC_{71}BM$ from 3:3 to 3:12 (w/w) were fabricated to optimize the device fabrication process. In addition, we fabricated devices with different concentrations of processing additives in CF from 1.5 to 2.5 vol.% such as DPE and 1,8-diiodooctane(DIO). The data are summarized in Table S3. The optimum blend ratio of donor to $PC_{71}BM$ and the optimum concentration of DPE in CF were determined as 3:8 and 2.0 vol.%, respectively. Fig. 5 **(a)** shows the current density as a function of the voltage of the OSCs showing the best PCE under 1.0 sun illumination (inset: dark conditions) at the optimum blend ratio of donor and $PC_{71}BM$ and optimum concentration of processing additives. The photovoltaic parameters are summarized in Table 2.

Even though the optical and electrochemical properties of **IDTT-HT-CMCN** are almost identical to those of **IDTT-CMCN**, the presence of the **HT** group between **IDTT** and **CMCN** improves the PCE from 0.36 to 2.11%. The enhancement of the PCE is presumably due to the increase in the solubility of **IDTT-HT-CMCN** in CF (up to 10 mg/mL). The device containing DIO as a processing additive showed a significant enhancement in PCE from 2.11% to 5.93%. The improvement of the PCE mainly resulted from a 122% increase in the $J_{sc}$. Similarly, the PCE of the device with DPE as a processing additive exhibited the best PCE of 7.60%. The $R_s$ data also agree well with the device data. The calculated $J_{sc}$ values based on incident photon-to-current efficiency (IPCE) curves (Fig. 5 **(b)**) showed very good agreement with the $J_{sc}$ data measured from the devices under 1.0 sun illumination. Interestingly, the PCEs of the devices treated with CF vapor for 30 and 60 s in the glove box were decreased (See Table S3).

Hole- and electron-only devices with a structure of ITO/PEDOT:PSS (40 nm)/**IDTT-HT-CMCN**:$PC_{71}BM$ (3:8 by weight, 2.0 vol.% DPE, 60 nm)/Au (50 nm) and ITO/ZnO (20 nm)/**IDTT-HT-CMCN**:$PC_{71}BM$ (3:8 by weight, 2.0 vol.% DPE, 60 nm)/LiF (1 nm)/Ag (100 nm), respectively, have been fabricated and tested to investigate the charge transporting properties. As shown in Fig. S5, the *J-V* curves showed a characteristic of space charge limited current (SCLC) and can be expressed by the Mott-Gurney law [41];

$$J = \frac{9}{8}\varepsilon_0\varepsilon_r\mu\frac{E^2}{L}$$

where $J$ is the current density, $\mu$ is the charge mobility, $E$ is the electric field, $\varepsilon_0\varepsilon_r$ is the permittivity the active layer, and L is the thickness of the active layer. We calculated the charge mobility using the permittivity of 3.0 for the active layer. εr = 3.9The hole and electron mobility of the device were $1.43 \times . 10^{-3}$ and $2.10 \times . 10^{-3}$ $cm^2V^{-1}s^{-1}$, respectively. Notably, the electron mobility of the active layer is higher than that of hole mobility.

As shown in the UV–Vis spectra of the active layers (Fig. S6), the absorbance at 400–490 nm and 560–750 nm of the active layer with additives are higher than that of the active layer without additives. This is one of the reasons why the devices with additives exhibit higher PCEs than the devices without additives. The morphologies of the active layers based on **IDTT-HT-CMCN** were investigated by transmission electron microscopy (TEM) (Fig. 6). The active layer without additives showed significant phase separation and aggregation (Fig. 6 **(a)**). However, the active layers with DIO and DPE (Fig. 6 **(a)**, **(b)**) exhibited better nanoscale phase separation and bicontinuous interpenetrating networks. It was observed that the active layer with DPE showed the best nanoscale phase separated morphology. Thus, favorable nanoscale phase separation in the active layer can result in a higher PCE of the related OSC through efficient charge separation and transport [42]. Based on the grazing incidence wide angle X-ray scattering (GIWAXS) of **IDTT-HT-CMCN** (Fig. S7), we concluded that the **IDTT-HT-CMCN** films do not show any packing behavior.

## 3. Conclusion

In this work, two novel conjugated small-molecule-donor materials based on **IDTT** and **CMCN**, labeled **IDTT-CMCN** and **IDTT-HT-CMCN**, were developed for organic solar cells. The electron-accepting **CMCN** group, when combined with **IDTT,** can effectively form a powerful push-pull structure that induces effective ICT and enhanced optical absorption. In comparison with **IDTT-CMCN**, **IDTT-HT-CMCN** has **HT** as a π-bridge unit between the **IDTT** and **CMCN** moieties to increase the solubility and extend the π-conjugation length. The PCEs of the devices based on **IDTT-CMCN** were poor, at around 0.25–0.45%. Even though devices containing DPE as a processing additive were fabricated, the PCEs were not improved. **IDTT-HT-CMCN** with the hexylthiophene ring as a π-bridge showed a smaller band gap and better solubility, thus resulting in a PCE as high as 7.60% with a short circuit current of 12.7 $mA/cm^2$, open circuit voltage of 0.94 V, and fill factor of 63.8%.

## Acknowledgement

This research was supported by the New & Renewable Energy Core Technology Program of the Korea Institue of Energy Technology Evaluation and Planning (KETEP) under program number (20153010140030, 2018201010636).

## Appendix A. Supplementary data

Supplementary data to this article can be found online at https://doi.org/10.1016/j.dyepig.2018.12.060.

## References

[1] Yu G, Gao J, Hummelen JC, Wudl F, Heeger AJ. Polymer photovoltaic cells: enhanced efficiencies via a network of internal donor-acceptor heterojunctions. Science (80- ) 1995;270:1789–91.
[2] Günes S, Neugebauer H, Sariciftci NS. Conjugated polymer-based organic solar cells. Chem Rev 2007;107:1324–38.
[3] Cheng YJ, Yang SH, Hsu CS. Synthesis of conjugated polymers for organic solar cell applications. Chem Rev 2009;109:5868–923.
[4] Kan B, Li M, Zhang Q, Liu F, Wan X, Wang Y, et al. A series of simple oligomer-like small molecules based on oligothiophenes for solution-processed solar cells with high efficiency. J Am Chem Soc 2015;137:3886–93.
[5] He Z, Xiao B, Liu F, Wu H, Yang Y, Xiao S, et al. Single-junction polymer solar cells with high efficiency and photovoltage. Nat Photon 2015;9:174–9.
[6] Liu Y, Zhao J, Li Z, Mu C, Ma W, Hu H, et al. Aggregation and morphology control enables multiple cases of high-efficiency polymer solar cells. Nat Commun 2014;5:5293.
[7] Wan J, Xu X, Zhang G, Li Y, Feng K, Peng Q. Highly efficient halogen-free solvent processed small-molecule organic solar cells enabled by material design and device engineering. Energy Environ Sci 2017;10:1739–45.
[8] Kyaw AKK, Wang DH, Gupta V, Zhang J, Chand S, Bazan GC, et al. Efficient solution-processed small-molecule solar cells with inverted structure. Adv Mater 2013;25:2397–402.
[9] Shi Q, Cheng P, Li Y, Zhan X. A solution processable D-A-D molecule based on thiazolothiazole for high performance organic solar cells. Adv Energy Mater 2012;2:63–7.
[10] Bai H, Wang Y, Cheng P, Li Y, Zhu D, Zhan X. Acceptor–donor–acceptor small molecules based on indacenodithiophene for efficient organic solar cells. ACS Appl Mater Interfaces 2014;6:8424–33.
[11] Kan B, Zhang Q, Li M, Wan X, Ni W, Long G, et al. Solution-processed organic solar cells based on dialkylthiol-substituted benzodithiophene unit with efficiency near 10%. J Am Chem Soc 2014;136:15529–32.
[12] Zhou J, Zuo Y, Wan X, Long G, Zhang Q, Ni W, et al. Solution-processed and high-performance organic solar cells using small molecules with a benzodithiophene unit. J Am Chem Soc 2013;135:8484–7.
[13] Sun K, Xiao Z, Lu S, Zajaczkowski W, Pisula W, Hanssen E, et al. A molecular nematic liquid crystalline material for high-performance organic photovoltaics. Nat Commun 2015;6:6013.
[14] Badgujar S, Lee GY, Park T, Song CE, Park S, Oh S, et al. High-performance small molecule via tailoring intermolecular interactions and its application in large-area organic photovoltaic modules. Adv Energy Mater 2016;6:1600228.
[15] Pola MK, Boopathi KM, Padhy H, Raghunath P, Singh A, Lin MC, et al. Synthesis of fluorinated benzotriazole (BTZ)- and benzodithiophene (BDT)-based low-bandgap conjugated polymers for solar cell applications. Dyes Pigments 2017;139:349–60.
[16] Zhou X, Lu J, Huang H, Yun Y, Li Z, You F, et al. Thieno[3,2-b]indole (TI) bridged A-π-D-π-A small molecules: synthesis, characterizations and organic solar cell applications. Dyes Pigments 2019;160:16–24.
[17] Van Der Poll TS, Love JA, Nguyen TQ, Bazan GC. Non-basic high-performance molecules for solution-processed organic solar cells. Adv Mater 2012;24:3646–9.
[18] Ni W, Li M, Liu F, Wan X, Feng H, Kan B, et al. Dithienosilole-based small-molecule organic solar cells with an efficiency over 8%: investigation of the relationship between the molecular structure and photovoltaic performance. Chem Mater 2015;27:6077–84.
[19] Chen X, Sun Y, Wang Z, Gao H, Lin Z, Ke X, et al. Dithienosilole-based small molecule donors for efficient all-small-molecule organic solar cells. Dyes Pigments 2018;158:445–50.
[20] Chen X, Feng H, Lin Z, Jiang Z, He T, Yin S, et al. Impact of end-capped groups on the properties of dithienosilole-based small molecules for solution-processed organic solar cells. Dyes Pigments 2017;147:183–9.
[21] Zhang Q, Kan B, Liu F, Long G, Wan X, Chen X, et al. Small-molecule solar cells with efficiency over 9%. Nat Photon 2015;9:35–41.
[22] Zhang Q, Wang Y, Kan B, Wan X, Liu F, Ni W, et al. A solution-processed high performance organic solar cell using a small molecule with the thieno[3,2-b]thiophene central unit. Chem Commun 2015;51:15268–71.
[23] Deng D, Zhang Y, Zhang J, Wang Z, Zhu L, Fang J, et al. Fluorination-enabled optimal morphology leads to over 11% efficiency for inverted small-molecule organic solar cells. Nat Commun 2016;7:13740.
[24] Xu YX, Chueh CC, Yip HL, Ding FZ, Li YX, Li CZ, et al. Improved charge transport and absorption coefficient in indacenodithieno[3,2-b]thiophene-based ladder-type polymer leading to highly efficient polymer solar cells. Adv Mater 2012;24:6356–61.
[25] Bai H, Wu Y, Wang Y, Wu Y, Li R, Cheng P, et al. Nonfullerene acceptors based on extended fused rings flanked with benzothiadiazolylmethylenemalononitrile for polymer solar cells. J Mater Chem A 2015;3:20758–66.
[26] Lin Y, Wang J, Zhang Z-G, Bai H, Li Y, Zhu D, et al. An electron acceptor challenging fullerenes for efficient polymer solar cells. Adv Mater 2015;27:1170–4.
[27] Zhao W, Qian D, Zhang S, Li S, Inganäs O, Gao F, et al. Fullerene-Free polymer solar cells with over 11% efficiency and excellent thermal stability. Adv Mater 2016;28:4734–9.
[28] Zhao W, Li S, Yao H, Zhang S, Zhang Y, Yang B, et al. Molecular optimization enables over 13% efficiency in organic solar cells. J Am Chem Soc 2017;139:7148–51.
[29] Zhao F, Dai S, Wu Y, Zhang Q, Wang J, Jiang L, et al. Single-junction binary-blend nonfullerene polymer solar cells with 12.1% efficiency. Adv Mater 2017;29:1700144.
[30] Lin Y, Zhao F, He Q, Huo L, Wu Y, Parker TC, et al. High-performance electron acceptor with thienyl side chains for organic photovoltaics. J Am Chem Soc 2016;138:4955–61.
[31] Li S, Ye L, Zhao W, Zhang S, Mukherjee S, Ade H, et al. Energy-level modulation of small-molecule electron acceptors to achieve over 12% efficiency in polymer solar cells. Adv Mater 2016;28:9423–9.
[32] Xie D, Liu T, Gao W, Zhong C, Huo L, Luo Z, et al. A novel thiophene-fused ending group enabling an excellent small molecule acceptor for high-performance fullerene-free polymer solar cells with 11.8% efficiency. Sol RRL 2017;1:1700044.
[33] Dai S, Zhao F, Zhang Q, Lau T-K, Li T, Liu K, et al. Fused nonacyclic electron acceptors for efficient polymer solar cells. J Am Chem Soc 2017;139:1336–43.
[34] Yao H, Ye L, Hou J, Jang B, Han G, Cui Y, et al. Achieving highly efficient nonfullerene organic solar cells with improved intermolecular interaction and open-circuit voltage. Adv Mater 2017;29:1700254.
[35] Yang Y, Zhang ZG, Bin H, Chen S, Gao L, Xue L, et al. Side-Chain isomerization on

an n-type organic semiconductor ITIC acceptor makes 11.77% high efficiency polymer solar cells. J Am Chem Soc 2016;138:15011–8.
[36] Wang HC, Tang LM, Zuo L, Chen H, Xu YX. Investigating the crystalline nature, charge transport properties and photovoltaic performances of ladder-type donor based small molecules. RSC Adv 2015;5:80677–81.
[37] Intemann JJ, Yao K, Ding F, Xu Y, Xin X, Li X, et al. Enhanced performance of organic solar cells with increased end group dipole moment in indacenodithieno [3,2-b]thiophene-based molecules. Adv Funct Mater 2015;25:4889–97.
[38] Yang D, Sasabe H, Sano T, Kido J. Low-band-gap small molecule for efficient organic solar cells with a low energy loss below 0.6 eV and a high open-circuit voltage of over 0.9 v. ACS Energy Lett 2017;2:2021–5.
[39] Zhang XH, Chen BJ, Lin XQ, Wong OY, Lee CS, Kwong HL, et al. A new family of red dopants based on chromene-containing compounds for organic electroluminescent devices. Chem Mater 2001;13:1565–9.
[40] Lee J, Aizawa N, Yasuda T. Isobenzofuranone- and chromone-based blue delayed fluorescence emitters with low efficiency roll-off in organic light-emitting diodes. Chem Mater 2017;29:8012–20.
[41] Bagui A, Iyer SSK. Increase in hole mobility in poly (3-hexylthiophene-2,5-diyl) films annealed under electric field during the solvent drying step. Org Elect Phy Mater Appl 2014;15:1387–95.
[42] Ye L, Zhang S, Zhao W, Yao H, Hou J. Highly efficient 2D-conjugated benzodithiophene-based photovoltaic polymer with linear alkylthio side chain. Chem Mater 2014;26:3603–5.